

# Synaptic Activation of T-Type $\text{Ca}^{2+}$ Channels Via mGluR Activation in the Primary Dendrite of Mitral Cells

Jamie Johnston and Kerry R. Delaney

*J Neurophysiol* 103:2557-2569, 2010. First published 13 January 2010; doi:10.1152/jn.00796.2009

**You might find this additional info useful...**

---

This article cites 49 articles, 31 of which can be accessed free at:

<http://jn.physiology.org/content/103/5/2557.full.html#ref-list-1>

This article has been cited by 3 other HighWire hosted articles

**Prolonged Postinhibitory Rebound Firing in the Cerebellar Nuclei Mediated by Group I Metabotropic Glutamate Receptor Potentiation of L-Type Calcium Currents**

Nan Zheng and Indira M. Raman

*J. Neurosci.*, July 13, 2011; 31 (28): 10283-10292.

[\[Abstract\]](#) [\[Full Text\]](#) [\[PDF\]](#)

**Basal sympathetic activity generated in neonatal mouse brainstem–spinal cord preparation requires T-type calcium channel subunit  $\alpha 1H$**

Chien-Chang Chen, Yu-Pei Fan, Hee-Sup Shin and Chun-Kuei Su

*Exp Physiol*, May 1, 2011; 96 (5): 486-494.

[\[Abstract\]](#) [\[Full Text\]](#) [\[PDF\]](#)

**Differential Binding of Calmodulin to Group I Metabotropic Glutamate Receptors Regulates Receptor Trafficking and Signaling**

Kyu Yeong Choi, Seungsoo Chung and Katherine W. Roche

*J. Neurosci.*, April 20, 2011; 31 (16): 5921-5930.

[\[Abstract\]](#) [\[Full Text\]](#) [\[PDF\]](#)

Updated information and services including high resolution figures, can be found at:

<http://jn.physiology.org/content/103/5/2557.full.html>

Additional material and information about *Journal of Neurophysiology* can be found at:

<http://www.the-aps.org/publications/jn>

---

This information is current as of August 29, 2011.

# Synaptic Activation of T-Type $\text{Ca}^{2+}$ Channels Via mGluR Activation in the Primary Dendrite of Mitral Cells

Jamie Johnston and Kerry R. Delaney

Department of Biology, University of Victoria, Victoria, British Columbia, Canada

Submitted 25 August 2009; accepted in final form 13 January 2010

**Johnston J, Delaney KR.** Synaptic activation of T-type  $\text{Ca}^{2+}$  channels via mGluR activation in the primary dendrite of mitral cells. *J Neurophysiol* 103: 2557–2569, 2010. First published January 13, 2010; doi:10.1152/jn.00796.2009. Mitral cells are the primary output of the olfactory bulb, projecting to many higher brain areas. Understanding how mitral cells process and transmit information is key to understanding olfactory perception. Mitral dendrites possess high densities of voltage-gated channels, are able to initiate and propagate orthodromic and antidromic action potentials, and release neurotransmitter. We show that mitral cells also possess a low-voltage-activated T-type  $\text{Ca}^{2+}$  current. Immunohistochemistry shows strong Cav3.3 labeling in the primary dendrite and apical tuft with weaker staining in basal dendrites and no staining in somata. A low-voltage-activated  $\text{Ca}^{2+}$  current activates from  $-68$  mV, is blocked by  $500 \mu\text{M}$   $\text{Ni}^{2+}$  and  $50 \mu\text{M}$  NNC 55-0396, but is insensitive to  $50 \mu\text{M}$   $\text{Ni}^{2+}$  and  $500 \mu\text{M}$  isradipine. 2-photon  $\text{Ca}^{2+}$  imaging shows that T channels are functionally expressed in the primary dendrite where their activity determines the resting  $[\text{Ca}^{2+}]$  and are responsible for subthreshold voltage-dependent  $\text{Ca}^{2+}$  changes previously observed in vivo. Application of the group 1 mGluR agonist dihydroxyphenylglycine (DHPG) ( $50 \mu\text{M}$ ) robustly upregulates T-channel current in the primary and apical tuft dendrite. Olfactory nerve stimulation generates a long-lasting depolarization, and we show that mGluRs recruit T channels to contribute  $\sim 36\%$  of the voltage integral of this depolarization. The long-lasting depolarization results in sustained firing and block of T channels decreased action potential firing by  $84.1 \pm 4.6\%$ . Therefore upregulation of T channels by mGluRs is required for prolonged firing in response to olfactory nerve input.

## INTRODUCTION

The olfactory nerve projects directly to the olfactory bulb where it synapses in spherical structures of dense neuropil, called glomeruli. Mitral cells, the main output neurons of the olfactory bulb, send their primary dendrites  $\sim 500 \mu\text{m}$  across the external plexiform layer to a single glomerulus where it is excited given sufficient input from the olfactory nerve (Gire and Schoppa 2009).

Like many other neurons, the dendrites of mitral cells are active, possessing a range of voltage-gated channels including: classic Nav channels, high-threshold Kv channels (Bischofberger and Jonas 1997), persistent sodium channels (Balu and Strowbridge 2007; Desmaisons et al. 1999), A-type  $\text{K}^+$  channels (Kollo et al. 2008), and high-threshold  $\text{Ca}^{2+}$  channels (Isaacson and Strowbridge 1998). A less common feature of mitral cell dendrites is that in addition to receiving synaptic input, they also form synapses (Price and Powell 1970) and release transmitter (Isaacson and Strowbridge 1998). Back-

propagating action potentials can release glutamate which both self excites and stimulates neighboring mitral cells in the same glomerulus. This feature is thought to synchronize firing in mitral cells that share a single glomerulus (Schoppa and Westbrook 2002). Mitral cells respond to strong olfactory nerve stimulation with a long-lasting depolarization (typically  $>1$  s) initiated in the distal portion of the primary dendrite (Carlson et al. 2000). This is a result of recurrent excitation among mitral cells, which activates *N*-methyl-D-aspartate (NMDA) and mGluR1 receptors (De Saint Jan and Westbrook 2007).

Unlike in vitro, the in vivo mitral cell membrane potential oscillates at subthreshold voltages with the same frequency as respiration (Cang and Isaacson 2003; Schaefer et al. 2006; Sobel and Tank 1993). With appropriate odor stimulation, the amplitude of these oscillations increases, resulting in bursts of action potentials on their crests. These subthreshold oscillations are accompanied by significant  $\text{Ca}^{2+}$  entry, which can be detected in vivo using  $\text{Ca}^{2+}$  imaging (Chrapak et al. 2001). In this previous study, we noted that in the absence of odor-evoked synaptic input, current injection that produced small perturbations of the membrane potential above and below rest resulted in corresponding changes in dendritic  $[\text{Ca}^{2+}]$ .

We show using immunohistochemistry, electrophysiology and 2-photon  $\text{Ca}^{2+}$  imaging, that mitral cells express dendritically localized T-type  $\text{Ca}^{2+}$  channels, probably the Cav3.3 isoform. Subthreshold  $\text{Ca}^{2+}$  entry in mitral cell primary dendrites is through these T channels. We also show that mGluR activation increases T-channel activity in the primary dendrite. This mGluR action on T channels generates a significant fraction of the depolarization from olfactory nerve stimulation and results in increased action potential firing.

## METHODS

### Brain slice preparation

Wild-type C57Blk/6J and B6.Cg-Tg (Thy1-YFP) 16Jrs mice (Feng et al. 2000) aged P14–24 (postnatal days) were anesthetized with urethane ( $\sim 35$  mg) and decapitated. The brain was removed into iced slicing artificial cerebrospinal fluid (ACSF) containing (in mM) 2.5 KCl, 10 glucose, 1.25  $\text{NaH}_2\text{PO}_4$ , 250 sucrose, 26  $\text{NaHCO}_3$ , 4  $\text{MgCl}_2$ , and 0.1  $\text{CaCl}_2$ . The olfactory bulb hemispheres were separated and individually mounted dorsal side down on the stage of a Leica VT1000 S, and 250 to 300- $\mu\text{m}$ -thick horizontal sections were cut. Slices were transferred to the recording ACSF, which contained (in mM) 125 NaCl, 2.5 KCl, 10 glucose, 1.25  $\text{NaH}_2\text{PO}_4$ , 3 myo-inositol, 26  $\text{NaHCO}_3$ , 1  $\text{MgCl}_2$ , and 2  $\text{CaCl}_2$  (pH 7.4), incubated at  $37^\circ\text{C}$  for 1 h and then maintained at room temperature until required.

### Electrophysiology

For recording, a slice was transferred to a JG-23 ultra-quiet imaging chamber attached to a PM-1 resistive heating platform (Warner

Address for reprint requests and other correspondence: K. R. Delaney, Dept. of Biology, University of Victoria, Victoria, B.C. Canada V8W 3N5 (E-mail: kdelaney@uvic.ca).

Instruments, Hamden CT). The slices were perfused with 34–36°C ACSF at a rate of ~1–2 ml/min. Mitral cell bodies were identified by their size and location in the mitral cell layer using an Olympus BX51WI microscope fitted with a CCD camera and oblique condenser. Patch pipettes were pulled from thick-walled borosilicate tubing (BF150×86×7.5, Sutter Instruments) and whole cell recordings performed with an EPC10 dual headstage amplifier (HEKA, Lambrecht, Germany). For voltage-clamp recordings, the pipette contained (in mM) 110 CsCH<sub>3</sub>SO<sub>3</sub>, 10 glutamate, 10 tetraethyl ammonium (TEA), 5 4-aminopyridine (4-AP), 10 HEPES, 10 phosphocreatine, 2 Mg.ATP, 0.3 Na.GTP, and 0.15 Ca<sup>2+</sup> buffer (EGTA- or Ca<sup>2+</sup>-sensitive dye) pH 7.2 with CsOH and had series resistances of 7–20 MΩ, which was compensated 70–80% with 10-μs lag. For current clamp, pipettes contained (in mM) 110 KCH<sub>3</sub>SO<sub>4</sub>, 8 KCl, 10 glutamate, 10 HEPES, 10 phosphocreatine, 2 Mg.ATP, and 0.3 Na.GTP, pH 7.2 with KOH and had series resistances of 7–20 MΩ, which was compensated by the bridge balance circuitry. Electrophysiological data were sampled at 20 kHz and filtered at 3–5 kHz. For current recordings, *p/n* leak subtraction was performed to minimize uncompensated capacitive artifacts. All recordings were performed ≥20 min after break-through to allow dialysis of the large dendritic compartments.

#### Alternate solutions for isolating Ca<sup>2+</sup> currents

For the voltage-clamp experiments in Fig. 3, the ACSF was modified to isolate Ca<sup>2+</sup> currents from all other conductances. NaCl was replaced with TEA-Cl, 40 μM 6,7-dinitroquinoxaline-2,3-dione (DNQX), 40 μM 2-amino-5-phosphonovaleric acid (APV), and 20 μM bicuculline were included to prevent synaptic currents, and 0.5 μM tetrodotoxin was added to ensure voltage-gated Na<sup>+</sup> currents were absent. In two cells, we tried to ameliorate the space-clamp problem by blocking the high-voltage-activated N-type and L-type Ca<sup>2+</sup> channels with conotoxin GVIIA and isradipine. Although this resulted in more “transient-like” currents (compare Fig. 3*B*, *ii* with *i*), it did not prevent loss of clamp, so we did not pursue this further. These cells were included in the pooled data as the LVA current appeared unaffected.

#### Alternate solutions for imaging resting [Ca<sup>2+</sup>]

In experiments where resting [Ca<sup>2+</sup>] was measured (Fig. 4), normal ACSF was used (with normal Na<sup>+</sup> to prevent possible reversal of the Na<sup>+</sup>-Ca<sup>2+</sup> exchange) with the addition of synaptic blockers (40 μM DNQX, 40 μM APV, 20 μM Bic) and 2 mM CsCl to block *I<sub>n</sub>* and *K<sub>ir</sub>* currents, improving clamp for negative steps. A 3 M KCl agarose bridge reference electrode was used in all experiments. Because the ionic composition of the solutions varied, all stated voltages have been corrected for their liquid junction potentials.

#### Electrical stimulation

In experiments with olfactory nerve stimulation, the recording pipette solution contained 30 μM Alexa 594 to locate the glomerulus to which the mitral dendrite projected. A bipolar electrode, constructed from theta glass (BT-150-10, Sutter Instruments, Novato CA) with a tip diameter of 3–4 μm, filled with ACSF, was placed in the olfactory nerve layer rostral to the glomerulus of interest. The pipette location was adjusted to give a robust response with a 0.1-mA 200-μs current pulse delivered by a SIU90 isolated current source (Cygnus Tech). The interstimulus interval between trials was ≥16 s.

#### Ca<sup>2+</sup> imaging

Cells were loaded by diffusion through the patch pipette with 150 μM of Ca<sup>2+</sup>-sensitive dye (either Ca-Green1, Fluo-4, or Rhod-2). For ratiometric measurements of [Ca<sup>2+</sup>] around resting membrane poten-

tials, Ca-Green was used as this dye has high affinity and brighter fluorescence at low [Ca<sup>2+</sup>], 30 μM Alexa 594 was included as the reference dye. Alexa 594 also served to help find and follow dendrites using low intensity laser illumination in the Fluo-4 experiments, since this indicator has a low fluorescence at resting [Ca<sup>2+</sup>]. Fluorescence was excited using 810-nm pulsed laser light generated by a Nd:YAG pumped Ti:sapphire laser system (Verdi 10W; MIRA Optima 900F; Coherent Laser, Santa Clara, CA). An *x-y* galvanometer mirror assembly scanned the beam across the sample through a ×40, 0.8 numerical aperture water-dipping lens (Olympus). Ca<sup>2+</sup> dye fluorescence signals were detected using a Hamamatsu H7422P-40 photomultiplier, and for ratiometric measurements, the Ca<sup>2+</sup>-insensitive fluorescence was simultaneously detected with a Hamamatsu (Cambridge Technology) HGT52-05 photomultiplier using a customized Olympus BX51WI microscope. Fluorescence signals were spectrally separated using appropriate combinations of filters and a dichroic mirror. A Macintosh computer (Apple, Cupertino CA) equipped with a NI PCI6111 A/D converter was used to acquire fluorescence signals (600-kHz to 1.25-MHz sampling rate) and to output scan-wave signals simultaneously with acquisition. Hardware control, image acquisition, and analysis were written in-house using Igor Pro (Wavemetrics, Eugene OR). External C++ routines were linked to the Igor interface to accelerate some display and analysis functions. Imaging was performed by scanning small rectangular scan areas that encompassed a length of dendrite and an area of background. Dendrites were aligned along the horizontal axis of the scan using a hardware-based scan rotation device with bidirectional scanning in the horizontal axis to increase scanning rates. Frame rates in the range of 30–150 Hz were typically used.

Polygonal regions of interest (ROIs) were drawn around dendritic structures, and the signal was corrected by subtraction of background fluorescence from adjacent nonfilled tissue. For experiments using a single dye, fluorescence was normalized by dividing by the average fluorescence during a period of inactivity (normally the 1st second of each trial). For the green/red (G/R) ratiometric measurements in Fig. 4, red and green dye fluorescence was corrected for background fluorescence and average pixel intensity within the ROI was calculated for each frame. The time-dependent red fluorescence signal was polygonally smoothed (Savitzky-Golay, 11-point window) prior to calculating the G/R ratio. The average Ca<sup>2+</sup> fluorescence values measured in the last 500 ms prior to voltage steps was used to allow equilibration of the Ca<sup>2+</sup> across the dendritic compartment.

#### Immunohistochemistry

Animals were deeply anesthetized by injection of an overdose of urethane and perfused prior to respiratory failure with 6–10 ml of PBS through the left ventricle of the heart returning to exit through an incision in the right atrium. This was followed by perfusion with 6–10 ml of 4% PFA (pH 7.4). The brain was then removed and placed in 4% PFA overnight at 4°C, then transferred to 30% sucrose PBS where it was stored until used. For sectioning, the brain was submersed in Tissue Tek (Sakura, Zoeterwoude Holland) and cryostat frozen sections 20–25 μm thick were then adhered to poly-L-lysine-coated slides (Newcomer Supply, Middleton WI). Sections were rinsed 3 × 10 min in PBS and then incubated in blocking buffer for 1–2 h at room temperature. The blocking buffer contained 4% donkey serum, 2% DMSO, 0.2% TWEEN in PBS. The primary antibody solution was applied at room temperature for ≥16 h. The primary antibody solution contained 1% donkey serum, 0.1% sodium azide, 2% DMSO, 0.2% TWEEN, and 1:200 to 1:1,000 dilution of primary antibody. Sections were rinsed 3 × 10 min in PBS and incubated for ≥2h in the secondary antibody solution, which contained: 1% donkey serum, 2% DMSO, 0.2% TWEEN, and 1:500 Alexa 647 donkey-anti-rabbit (Molecular Probes, Invitrogen). Sections were then rinsed 6 × 10 min in PBS and mounted with Immu-mount (Thermo Scientific). Fluorescence images were collected with either a Nikon Eclipse

TE2000-U confocal or a Olympus BX51 confocal with excitation at 488 and 633 nm.

### Drugs and solutions

All chemicals were obtained from Sigma except DNQX and APV, which were obtained from Cedarlane Labs and  $\omega$ -CTX from Alomone (Jerusalem, Israel). Anti-Cav3.1 and anti-Cav3.3 were gifts from Drs. T. Snutch (University of British Columbia) and G. Zamponi (University of Calgary).

### Statistics

All data are expressed as means  $\pm$  SE, with *t*-test or ANOVA used to assess significance, where appropriate.

## RESULTS

### $[\text{Ca}^{2+}]$ in mitral cell dendrites is sensitive to membrane potential near rest

The membrane potential of mitral cells *in vivo* oscillates at subthreshold potentials with the same frequency as respiration (Cang and Isaacson 2003; Schaefer et al. 2006). These subthreshold oscillations are accompanied by increases in  $[\text{Ca}^{2+}]$  (Charpak et al. 2001). To probe the channels contributing to this subthreshold influx, we used acute slices that allow stable electrophysiological recordings, high-resolution  $\text{Ca}^{2+}$  imaging and most importantly pharmacological manipulations, which are not possible *in vivo*. *In vitro* the mitral cell membrane potential is relatively quiescent. To mimic the *in vivo* oscillations, we applied sine wave current injections with an amplitude that evoked peri-threshold oscillations of the membrane potential ( $213 \pm 22$  pA  $n = 19$ ). With ionotropic glutamate receptors blocked by 40  $\mu\text{M}$  APV and 40  $\mu\text{M}$  DNQX, we imaged the apical dendrite/tuft of 42 mitral cells dialyzed with  $\text{Ca}^{2+}$  indicator (150  $\mu\text{M}$  Rhod-2 or Fluo-4). In 25 of these cells, changes in  $[\text{Ca}^{2+}]$  were observed which corresponded with subthreshold voltage changes. The average  $\Delta F/F$  at the peak of the first oscillation was  $41 \pm 7\%$  ( $n = 16$ , Fig. 1A, cells that fired action potentials on the 1st oscillation were not included in this average). The peak  $\Delta F/F$  during the sinusoidal current injection was  $58.1 \pm 14.1\%$  of that evoked by a single back-propagating action potential imaged at the same location (Fig. 1B, *i* and *ii*,  $n = 4$ , all with Fluo-4). These responses are remarkably similar to changes that were observed *in vivo* with two-photon imaging from urethane-anesthetized rats (Charpak et al. 2001). Because synaptic sources of  $\text{Ca}^{2+}$  were blocked in these experiments, the subthreshold influx must be mediated by voltage-gated  $\text{Ca}^{2+}$  channels rather than voltage gating of NMDA receptors. In other neurons, two types of  $\text{Ca}^{2+}$  channels are known to be active at rest and contribute to the resting  $[\text{Ca}^{2+}]$  (Avery and Johnston 1996; Magee et al. 1996): The L-type Cav1.3 channel and all three members of the T-type (Cav3) family.

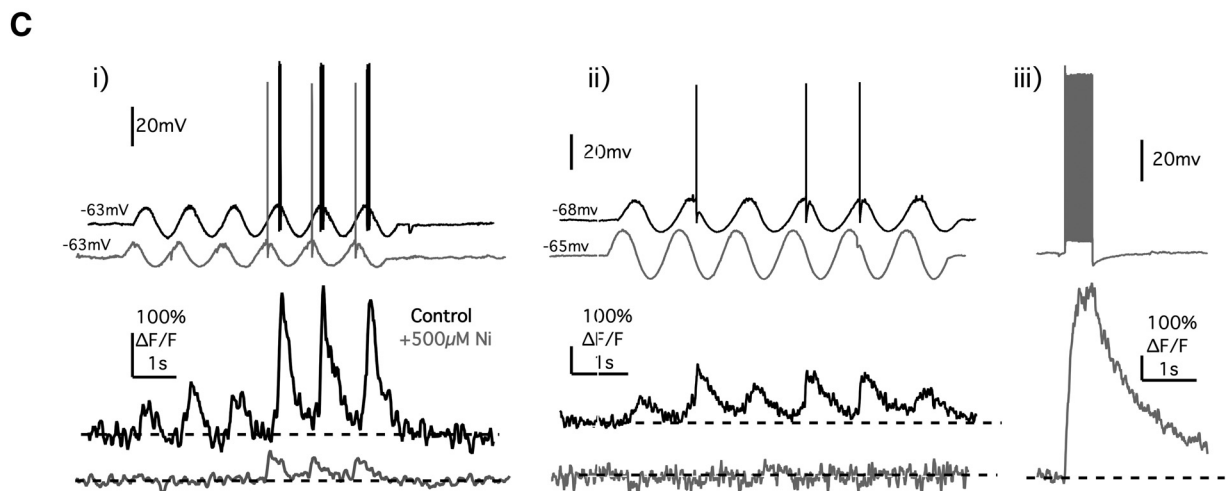
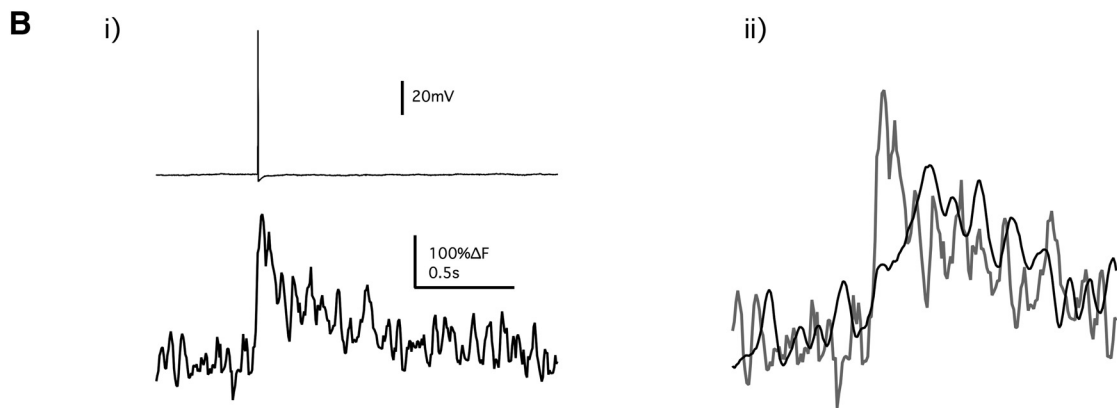
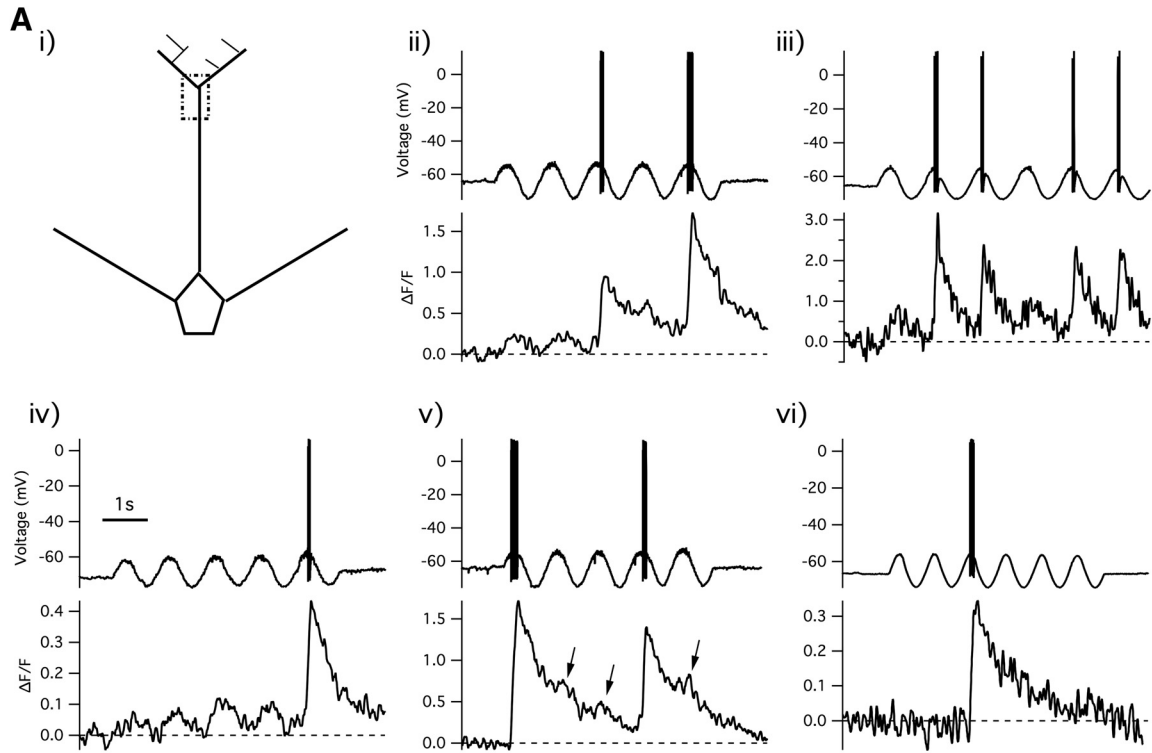
The pharmacological tools for investigating T-type channels are limited. High concentrations of  $\text{Ni}^{2+}$  can reduce other voltage-gated  $\text{Ca}^{2+}$  channels and NMDA receptors. Mibefradil has some specificity for T channels, but its metabolites are known to be effective blockers of L-type channels. NNC 55-0396 is a specific blocker that does not have active metabolites, but its block is voltage-dependent, so it is less effective at hyperpolarized potentials and like mibefradil is slow to washout (Huang et al. 2004). Consequently, a combination of

agents and experiments are needed to identify the contribution of T-type channels to subthreshold  $\text{Ca}^{2+}$  influx.

The  $\text{Ni}^{2+}$   $\text{IC}_{50}$  for Cav3.1 and Cav3.3 is  $\sim 250$   $\mu\text{M}$  (Lee et al. 1999), whereas that for Cav3.2 is  $\sim 12$   $\mu\text{M}$ . We ensured complete block of all three T-channels by using 500  $\mu\text{M}$   $\text{Ni}^{2+}$ . The subthreshold  $[\text{Ca}^{2+}]$  changes were abolished with application of 500  $\mu\text{M}$   $\text{Ni}^{2+}$  in all cells tested, whereas action potential mediated  $\text{Ca}^{2+}$  entry still occurred ( $n = 7$ , Fig. 1C). Although 500  $\mu\text{M}$   $\text{Ni}^{2+}$  will block T currents, it has been reported to attenuate some high-voltage-activated (HVA) and L-type currents (Avery and Johnston 1996; Brandt et al. 2003). To assess the effects of  $\text{Ni}^{2+}$  on HVA channels, we imaged the  $\text{Ca}^{2+}$  transient in response to a back-propagating action potential, recorded in 50  $\mu\text{M}$  APV, 40  $\mu\text{M}$  DNQX, and 50  $\mu\text{M}$  NNC 55-0396. 500  $\mu\text{M}$   $\text{Ni}^{2+}$  only reduced the action potential  $\text{Ca}^{2+}$  transient by  $24 \pm 9\%$  ( $n = 3$ ). The L-type blocker isradipine (500  $\mu\text{M}$ ), which is sufficient to block all L-type currents (Brandt et al. 2003; Koschak et al. 2001), had no effect on the dendritic subthreshold  $\text{Ca}^{2+}$  entry (control  $37 \pm 18\%$   $\Delta F/F$  vs. isradipine  $40 \pm 25\%$   $\Delta F/F$ ,  $n = 3$ ,  $P = 0.58$ , paired *t*-test). This supports the conclusion that L-type channels are not contributing to subthreshold  $\text{Ca}^{2+}$  influx. Together these data suggest T-type channels are the primary source of LVA  $\text{Ca}^{2+}$  influx into mitral cell primary dendrites.

### Cav3.3 is expressed in mitral cells

Recently the location of Cav3.x proteins has been reported in the majority of brain regions in the rat with the exception of the olfactory bulb (McKay et al. 2006). Using the same antibodies, we probed the subcellular distribution in the olfactory bulb (OB) with a specific interest in mitral cells. We took advantage of the expression of eYFP in mitral and external tufted cells in the B6.Cg-Tg (Thy1-YFP)16Jrs mouse strain (Feng et al. 2000) to determine whether antibody staining was co-localized to these cell types. Figure 2, A and B, shows Cav3.1 and Cav3.3 staining (red) in the YFP mice. In the OB, Cav3.1 is present in the granule cell layer and is particularly high in the outer portion of the external plexiform layer where it appears in somata and processes of small juxtglomerular cells. Cav3.1 immunoreactivity is absent from mitral cell somata and primary dendrites but is found in some external tufted cells (Fig. 2A, *inset*). Preferential localization of anti-Cav3.3 staining to dendrites of several neuronal subtypes is seen throughout the brain, including hippocampal pyramidal cells and cerebellar Purkinje neurons (McKay et al. 2006). This dendrite-specific localization of anti-Cav3.3 staining is also evident in the OB (Fig. 2B). Anti-Cav3.3 staining is exceptionally strong in the primary dendrites and distal tuft dendrites of mitral cells (Fig. 2, C and D). While some staining for Cav3.3 is seen in the granule layer, it is much weaker. Mitral secondary dendrites also showed evidence for Cav3.3 expression (Fig. 2D, white arrows), but clearly the predominant expression of this subtype is the apical dendritic compartment. Cav3.3 immunostaining was not observed in mitral cell somata. The epitope of the anti-Cav3.2 (rat) used by McKay et al. (2006) differs from mouse, and we were unable to reproduce the reported selective staining pattern with this antibody or with two different commercial products (Santa Cruz Biochemical and Alomone). However, electrophysiological experi-



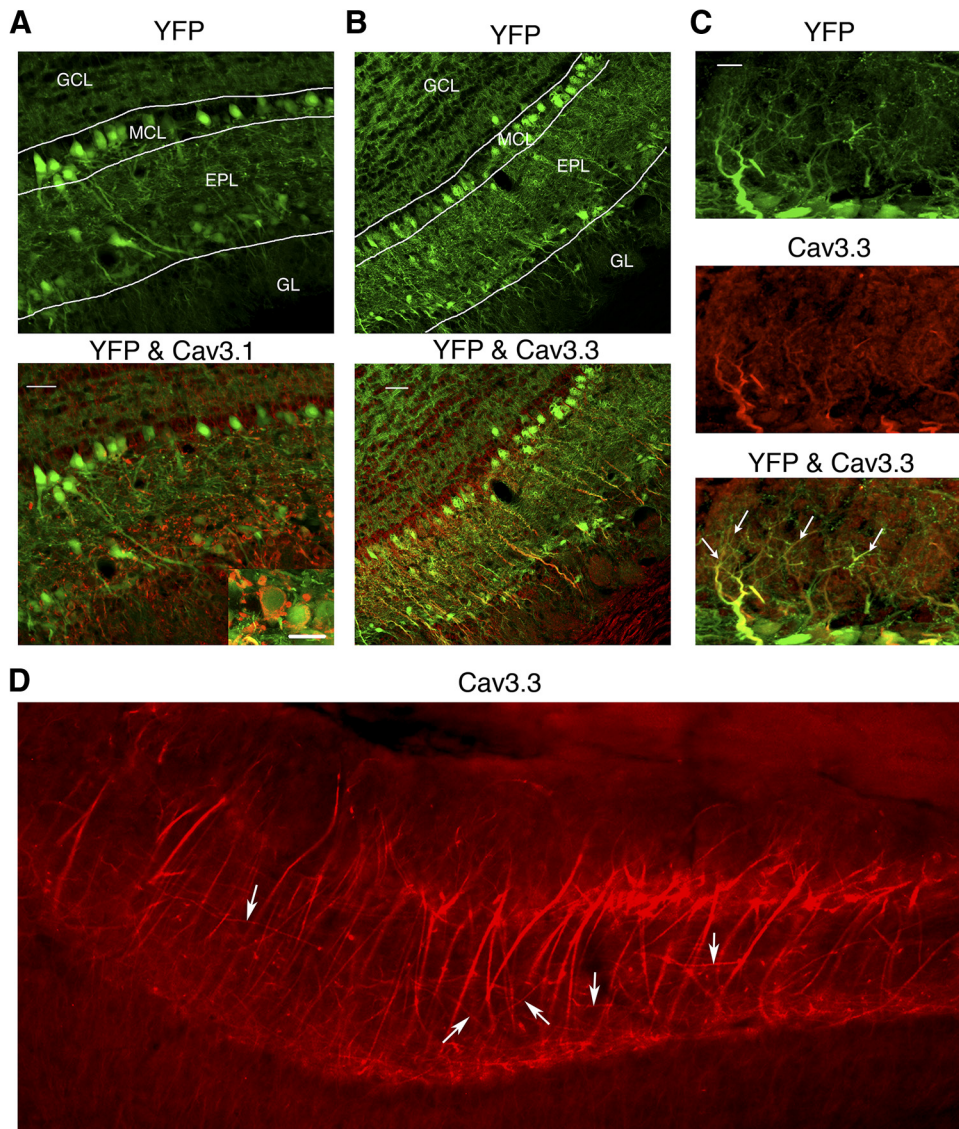


FIG. 2. Immunostaining of Cav3.1 and Cav3.3 in the olfactory bulb. *A*: horizontal olfactory bulb sections showing anti Cav3.1 staining (red) with YFP (green) expressed in mitral/tufted cells. Cav3.1 immunostaining is absent from the soma and primary dendrite of mitral cells but is seen in granule and juxtglomerular cells. Scale bar is 40  $\mu\text{m}$ . *Inset*: juxtglomerular neuron with Cav3.1 staining, scale bar is 20  $\mu\text{m}$ . *B*: Cav3.3 is strongly expressed in mitral primary dendrites (white arrows) and is also found in granule cell dendrites. Scale bar is 40  $\mu\text{m}$ . *C*: a magnified view of 2 glomeruli shows that Cav3.3 staining is present on the fine tuft branches (white arrows). Scale bar is 10  $\mu\text{m}$ . *D*: a low-power image of an olfactory bulb horizontal section stained with anti Cav3.3, note the strong staining in the thick primary dendrites of mitral cells extending into the glomeruli and weaker staining in the secondary dendrites (white arrows). GL, glomerular layer; EPL, external plexiform layer; MCL, mitral cell layer; GCL, granule cell layer.

ments described in the following text are not consistent with the expression Cav3.2 channels in mitral cells.

#### Voltage-clamp characterization of T-type Ca<sup>2+</sup> current

Having obtained evidence for a LVA Ca<sup>2+</sup> channel from imaging and immunohistochemistry, we used voltage clamp to confirm the presence of a LVA Ca<sup>2+</sup> current. To completely isolate the inward Ca<sup>2+</sup> currents from the Na<sup>+</sup> and K<sup>+</sup> currents, high external TEA-Cl (125 mM) was required, which replaced NaCl. 0.5  $\mu\text{M}$  TTX was included to ensure sodium channels were blocked, and 40  $\mu\text{M}$  DNQX, 40  $\mu\text{M}$  APV, and 20  $\mu\text{M}$  bicuculline were included to prevent fast synaptic currents.

The main apical trunk diameter of mitral cells is large and the characteristic length constant from soma to tuft is estimated to be 1,000–1,200  $\mu\text{m}$  (Djurisic et al. 2004). Therefore voltage control of apical compartments should be reasonable over voltages where the membrane behaves passively. However, once voltage-gated channels become active, space-clamp errors will result. These space-clamp errors are particularly problematic for voltage-activated inward currents; channels that open in the dendrite will cause distal locations to be more positive than the command voltage. In effect this results in a regenerative “Ca<sup>2+</sup> spike”, as seen in Fig. 3A (black arrow). The voltage control in distal locations is lost, so at “command” voltages where only LVA channels should be active, HVA

FIG. 1. Subthreshold Ca<sup>2+</sup> oscillations in the apical dendrite. *A*: example perithreshold sine wave current injections with simultaneous Ca<sup>2+</sup> imaging in the apical dendrite/tuft (*Ai*) from 5 different cells. *A, ii–iv*: subthreshold increases in Ca<sup>2+</sup> in 3 cells that did not spike on the 1st crest. *Av*: subthreshold increases were still detectable (black arrows) in cells that spiked on the 1st crest. *Avi*: an example from 1 of the 40% of cells that did not display any subthreshold Ca<sup>2+</sup> increases. *Bi*: peak Ca<sup>2+</sup> transients from subthreshold oscillations were  $58.1 \pm 14.1\%$  of those produced by a single back-propagating action potential imaged at the same location ( $n = 4$ ). *Bii*: the subthreshold increase in Ca<sup>2+</sup> is slower rising than action potential transients. *C, i* and *ii*: examples of the effects of 500  $\mu\text{M}$  Ni<sup>2+</sup> from 2 different cells, traces have been offset for clarity. Ni<sup>2+</sup> (gray traces) abolished the subthreshold Ca<sup>2+</sup> increases in all 7 cells tested, whereas action potential mediated Ca<sup>2+</sup> entry still occurred. *Ciii*: step depolarization in the presence of Ni<sup>2+</sup> for the cell in *Cii*. N.B: all experiments using Ni<sup>2+</sup> had 40  $\mu\text{M}$  2-amino-5-phosphonovaleric acid (APV) and 40  $\mu\text{M}$  DNQX in control and voltages have been liquid junction potential corrected (–14 mV).

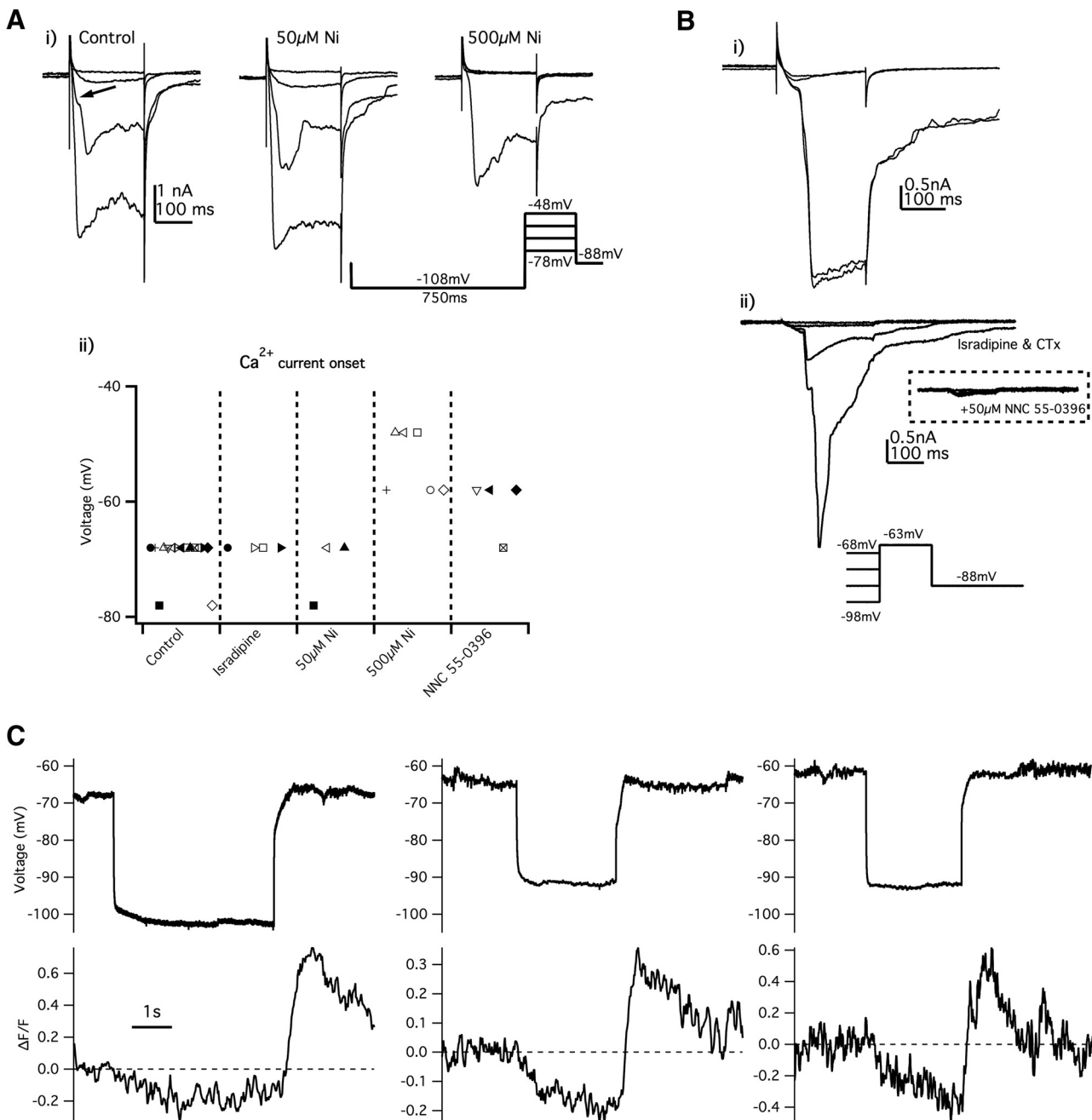


FIG. 3. A low-voltage-activated T-type  $\text{Ca}^{2+}$  current in mitral cells. *Ai*:  $\text{Ca}^{2+}$  currents from a single cell produced by the voltage protocol shown below the 500  $\mu\text{M}$   $\text{Ni}^{2+}$  trace. A current activates at  $-68$  mV in control conditions, and by  $-58$  mV, the current has become large enough for poor space clamp to result in loss of clamp (arrow).  $\text{Ni}^{2+}$  (50  $\mu\text{M}$ ) has no effect on the evoked currents; however, subsequent application of 500  $\mu\text{M}$   $\text{Ni}^{2+}$  prevents any calcium current from activating until  $-48$  mV. *Aii*: population data showing the voltage of  $\text{Ca}^{2+}$  current onset (defined with a threshold of 75 pA) for different conditions. Identical symbols show data from the same cell, e.g., the  $\blacksquare$  had a voltage onset of  $-78$  mV in control and application of 50  $\mu\text{M}$   $\text{Ni}^{2+}$  had no effect. *B, i* and *ii*: using a test potential of  $-58$  mV  $\text{Ca}^{2+}$  currents were evoked with 3-s prepulses to voltages between  $-98$  and  $-68$  mV (voltage protocol shown below *Bii*). As the prepulse potential was stepped positive the evoked  $\text{Ca}^{2+}$  current was attenuated eventually preventing loss of clamp by  $-83 \pm 1.5$  mV ( $n = 8$ ). The cell in *Bii* had 2  $\mu\text{M}$  CTx GVIIA and 500  $\mu\text{M}$  isradipine present, and the inset shows subsequent application of NNC 55-0396. *C*: the negatively shifted kinetics of T-channels normally bestows a rebound potential in neurons that is absent in mitral cells. Three examples of current-clamped mitral cells, a  $-300$ -pA current injection hyperpolarizes the neurons but no rebound potential is observed. However, a rebound in  $\text{Ca}^{2+}$  is observed in the apical dendrite, indicating the presence of low-voltage-activated (LVA) channels which have hyperpolarized inactivation kinetics ( $n = 6$ , similar location to that in Fig. 1).

channels will also be recruited. This precludes quantification of current magnitudes for construction of  $I$ - $V$  curves.

With the limitations described in the preceding text, we restricted quantification of drug effects to the voltage at which  $\text{Ca}^{2+}$  current started to activate. This was defined as the voltage at which  $\geq 75$  pA  $\text{Ca}^{2+}$  current first appeared. Blocking

LVA channels should shift the voltage onset to more depolarized potentials, where higher voltage-activated channels begin to open.  $\text{Ca}^{2+}$  currents were evoked by stepping to voltages between  $-78$  and  $-48$  mV from a prepotential of  $-108$  mV. As shown in Fig. 3A, a small slowly activating  $\text{Ca}^{2+}$  current is evoked at  $-68$  mV. At  $-58$  mV the current has increased and

an obvious deflection in the current is seen, indicating loss of voltage control (arrow in Fig. 3A). In all 20 cells tested, Ca<sup>2+</sup> currents were detected by -68 mV. Ca<sup>2+</sup> channels known to display hyperpolarized activation ranges include the L-type Cav1.3 (Xu and Lipscombe 2001) and the T-type Cav3 family (Klockner et al. 1999).

L-type antagonists (500  $\mu$ M isradipine,  $n = 4$ ) had no effect on the voltage onset of the LVA current (Fig. 3B) consistent with a lack of staining for Cav1.3 in the OB (Yuan et al. 2004). The voltage-onset of Ca<sup>2+</sup> current activation was insensitive to 50  $\mu$ M Ni<sup>2+</sup> ( $n = 3$ , Fig. 3, A and B) precluding involvement of Cav3.2 channels in the LVA current (Lee et al. 1999). However, 500  $\mu$ M Ni<sup>2+</sup> (which blocks both Cav3.1 and Cav3.3 channels) prevented any inward current from activating until steps to -58 or -48 mV (mean:  $-53 \pm 2$  mV,  $n = 6$ ,  $P < 0.05$ ), suggesting that either Cav3.1 and/or Cav3.3 mediate the LVA current. NNC 55-0396 is the most selective antagonist for T-type channels available that preferentially blocks T channels at concentrations  $\leq 100$   $\mu$ M (Huang et al. 2004). Application of 50  $\mu$ M NNC 55-0396 shifted the voltage onset of Ca<sup>2+</sup> current activation from approximately -68 to approximately -58 mV in three of the four cells tested (mean:  $-60 \pm 3$  mV,  $n = 4$ ,  $P < 0.05$ ). This is consistent with NNC 55-0396 blocking LVA channels, leaving higher voltage-activated channels intact. The lower efficacy of NNC 55-0396 is consistent with the voltage-dependent nature of this compound (Huang et al. 2004), which is less effective at hyperpolarized potentials.

A characteristic of T-type channels is that they have hyperpolarized steady-state inactivation curves (Klockner et al. 1999). Test to  $\geq -58$  mV steps from a prepotential of -98 mV evoked Ca<sup>2+</sup> currents that caused loss of clamp (Fig. 3, C and D). When the prepotential was brought more positive to  $-83 \pm 1.5$  mV ( $n = 8$ ), the evoked LVA Ca<sup>2+</sup> current was reduced preventing loss of clamp. Although poor space-clamp prevents quantification of steady-state inactivation curves, these data do indicate that the LVA Ca<sup>2+</sup> current starts to inactivate at negative potentials, consistent with its mediation by T channels.

Neurons that express T channels often exhibit a depolarizing rebound potential after hyperpolarization [e.g., thalamic neurons (Kim et al. 2001) and some juxtglomerular neurons (McQuiston and Katz 2001)], a phenomenon explained by the T channel's hyperpolarized activation and inactivation curves. With hyperpolarizing steps (-300 pA), a rebound potential was not observed in mitral cells (Fig. 3C) (Balu and Strowbridge 2007). However, when the Ca<sup>2+</sup> was imaged in the apical dendrite/tuft, a rebound in Ca<sup>2+</sup> was observed even though it was not accompanied by a rebound in voltage (Fig. 3C,  $n = 6$ ). This rebound in Ca<sup>2+</sup> is readily explained by removal of inactivation from a population of channels active at the resting membrane potential and indicates that in mitral cells, T channels have a window current around the resting membrane potential. Intriguingly, although a rebound in Ca<sup>2+</sup> is observed, a corresponding rebound in voltage is lacking. This discrepancy may be explained by the presence of an  $I_A$ -like K<sup>+</sup> current that has been shown to prevent rebound potentials after similar hyperpolarizing steps (Balu and Strowbridge 2007); additionally, the Ca<sup>2+</sup> current mediating the Ca<sup>2+</sup> rebound may be too small to evoke a rebound potential.

*T-type channels are active in dendrites and are regulated by group 1 mGluRs*

The voltage-clamp data demonstrate that mitral cells possess a LVA Ca<sup>2+</sup> current but do not indicate the subcellular location of these channels. The immunostaining suggests that the T-channel proteins are concentrated in the primary dendrite and apical tuft, are present in the secondary dendrites, and are absent from the soma.

To assess the location of active T channels, we used a ratiometric Ca<sup>2+</sup> imaging method (see METHODS) to compare the relationship between  $V_m$  and [Ca<sup>2+</sup>] in somata, secondary and primary apical/tuft dendrites. As we were measuring resting [Ca<sup>2+</sup>], normal ACSF was used (as opposed to the TEA solution) to prevent the possibility that any slowing or reversal of the Na<sup>+</sup>/Ca<sup>2+</sup> exchange would distort our measurements. However, the ACSF did have 2 mM CsCl present (which blocks inward rectifying K<sup>+</sup> currents and  $I_h$ ) to improve the clamp for the negative steps and 40  $\mu$ M APV, 40  $\mu$ M DNQX, and 20  $\mu$ M bicuculline to reduce background synaptic activity. By ensuring that NMDA-R were blocked, we also ensured that any Ni<sup>2+</sup>-dependent block of these receptors would not contribute to our results.

The resting [Ca<sup>2+</sup>] (at -64 mV) and the percentage drop in resting [Ca<sup>2+</sup>] on hyperpolarization to -94 mV were measured to assess the location of active T-channels. At -64 mV, T-channels will be the dominant voltage-dependent influx because they are the only active channels at this voltage (see Fig. 3). Furthermore, hyperpolarization will deactivate these channels, reducing the influx. Therefore a large drop in [Ca<sup>2+</sup>] on hyperpolarization from -64 mV is indicative of active T channels.

The resting [Ca<sup>2+</sup>] fluorescence (at -64 mV) appeared to be slightly higher in secondary versus primary dendrites ( $1.09 \pm 0.24$  vs.  $0.71 \pm 0.07$  G/R, Fig. 4B), and a proportionately larger drop in [Ca<sup>2+</sup>] was seen in the secondary dendrites on hyperpolarization ( $16.39 \pm 4.90\%$ ,  $n = 4$  vs.  $11.46 \pm 3.80\%$ ,  $n = 5$ , Fig. 4B, although these differences between primary and secondary dendrites were not statistically significant). The somata showed the highest resting [Ca<sup>2+</sup>] (G/R =  $1.19 \pm 0.13$ ) with the smallest [Ca<sup>2+</sup>] drop ( $5.20 \pm 2.96\%$ ,  $n = 3$ ). The lack of [Ca<sup>2+</sup>] sensitivity to voltage implies that the high somatic resting [Ca<sup>2+</sup>] is not due to influx through voltage-dependent channels. This discrepancy could be explained by a lower density of cytosolic extrusion mechanisms at the soma. More likely, the higher resting [Ca<sup>2+</sup>] could be an artifact of the seal leak. Even though it is small (32 pA at -64 mV for a 2-G $\Omega$  seal), the seal leak would artificially raise the resting [Ca<sup>2+</sup>] in a non-voltage dependent manner if measured close to the pipette.

As illustrated in the specific example chosen for presentation (Fig. 4A), not all mitral primary apical/tuft dendrites showed a prominent drop in [Ca<sup>2+</sup>] on hyperpolarization (when recorded in non-TEA containing ACSF). In the in vivo studies of Charpak et al. (2001), the sensitivity of resting [Ca<sup>2+</sup>] to membrane potential was seen to some degree in all cells where this was tested. This apparent lack of LVA Ca<sup>2+</sup> channel activity may be due to the relatively quiescent nature of an acute slice compared with the intact brain. Because mGluR1 receptors are strongly expressed in distal apical tuft dendrites

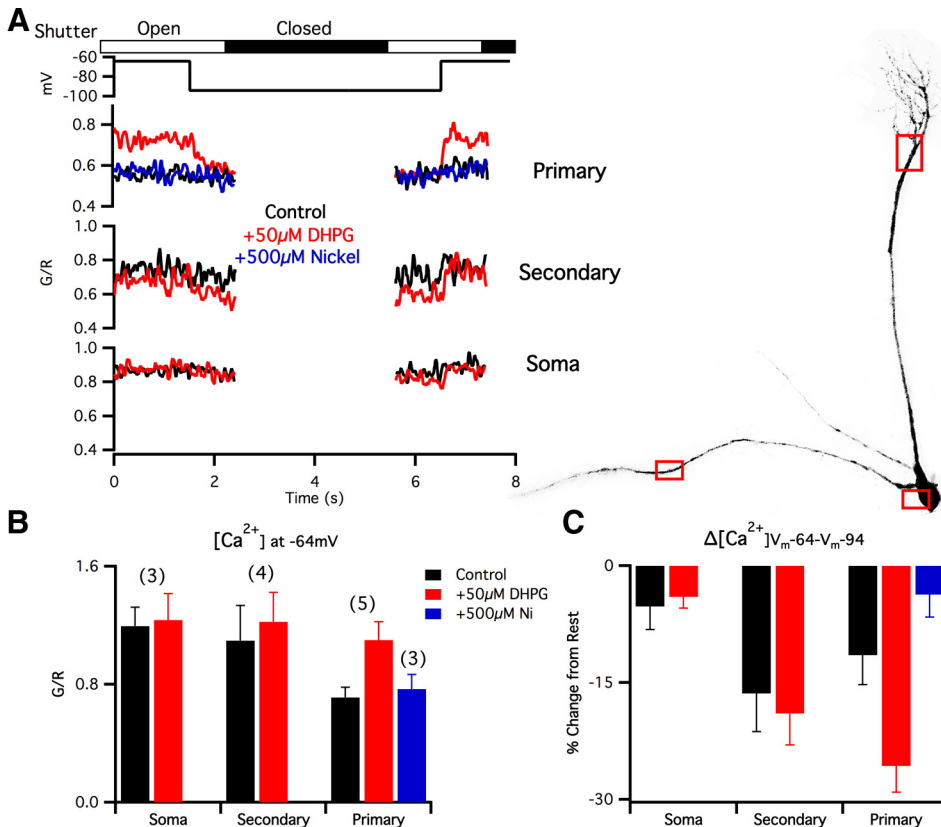


FIG. 4. Functional locations of T-type channels. *A, left*: example data from a single cell showing the experimental paradigm. Measurements were averaged from the 500 ms prior to voltage steps to ensure steady state was reached. The shutter was closed to limit photo-damage during the long trials. *Right*: example cell with imaging regions shown by red boxes. *B*: the resting  $[Ca^{2+}]$  shown as G/R for the 3 compartments in control (black), after 50  $\mu$ M DHPG (red), and after 500  $\mu$ M  $Ni^{2+}$  (blue). *C*: to demonstrate that a voltage-gated  $Ca^{2+}$  channel contributes to the resting  $[Ca^{2+}]$ , hyperpolarizing steps to  $-94$  mV were applied to deactivate channels, the percentage drop in G/R is shown in *C* for each compartment. N. B: red dye = 30  $\mu$ M Alexa-594, green dye = 150  $\mu$ M CaGreen-1. *n* is shown in parenthesis. APV, DNQX, and bicuculline were present in these experiments.

of mitral cells (van den Pol 1995), we hypothesized these may play a role in regulating T-channel activity.

Application of the group 1 mGluR agonist DHPG had the largest effect on the distal apical dendrite, significantly increasing the steady-state  $[Ca^{2+}]$  at  $-64$  mV (G/R = 0.71 in control vs. 1.10 in DHPG,  $P = 0.018$ ). Concurrently, the drop in  $[Ca^{2+}]$  on hyperpolarization was increased with DHPG application (11.46 vs. 25.68%,  $P = 0.020$ ,  $n = 5$ ), and all cells displayed a  $[Ca^{2+}]$  drop of  $>16\%$ . In the secondary dendrite, where resting  $[Ca^{2+}]$  was already high, activation of mGluRs had a smaller and more variable effect. The hyperpolarization-dependent  $[Ca^{2+}]$  drop was not significantly affected by DHPG,  $16.39 \pm 4.90$  versus  $18.95 \pm 4.04\%$  and the resting  $[Ca^{2+}]$  was only slightly affected with G/R increasing from  $1.09 \pm 0.24$  to  $1.22 \pm 0.20$  (Fig. 4, *B* and *C*,  $n = 4$ ,  $P = 0.67$ ). DHPG had no effect on the  $[Ca^{2+}]$  drop or the resting  $[Ca^{2+}]$  in the soma (Fig. 4, *B* and *C*,  $n = 3$ ). Application of 500  $\mu$ M  $Ni^{2+}$  occluded the effects of DHPG application on both resting  $[Ca^{2+}]$  and the  $[Ca^{2+}]$  drop in the primary apical/tuft dendrite (Fig. 4, *A-C*,  $n = 3$ ), indicating that DHPG acts to increase the effects of T-type channels on resting  $[Ca^{2+}]$ . Direct mGluR-induced  $Ca^{2+}$  release from intracellular stores, i.e., release that does not require  $Ca^{2+}$  influx through voltage-gated channels in the plasma membrane, is unlikely to be responsible for increased  $[Ca^{2+}]$  because changes in  $[Ca^{2+}]$  were sensitive to hyperpolarization, and occluded by  $Ni^{2+}$ . Unfortunately the long duration of experiments measuring  $Ca^{2+}$  in widely separated compartments of the same cell precluded testing the effects of  $Ni^{2+}$  in the secondary dendrites at the same time.

Our data show that mitral cells possess LVA-activated T-type channels (probably Cav3.3) in their dendrites and that these are regulated by mGluR in the primary dendrite. The

secondary dendrites also have LVA channels active at resting membrane potentials, but these do not appear to be regulated by mGluR.

Because mGluR activation plays a prominent role in the synaptic response of mitral cells (De Saint Jan and Westbrook 2007), we probed the role of T-channel modulation in the synaptic physiology of mitral cells.

#### *mGluR activation recruits LVA channels to contribute to the long-lasting depolarizations*

Mitral cells respond to olfactory nerve stimulation with long-lasting depolarizations (LLD) initiated in the distal portion of the primary dendrite (Carlson et al. 2000). The LLD is mediated in part by mGluR1 activation, the remainder being NMDA mediated (De Saint Jan and Westbrook 2007). The initial release of glutamate from the olfactory nerve excites mitral tuft dendrites inducing them to release glutamate from their own dendrites. This recurrent excitation results in saturation of transporters leading to activation of mGluRs.

Because Cav3.3 channels are located in the distal apical dendrite (Fig. 2C) and they are robustly unregulated by mGluR activation (Fig. 4), it seemed possible that they would be involved in the LLD. With 2 mM QX314 included to block action potential firing, application of the T-type channel antagonist mibefradil (10  $\mu$ M) reduced the integral of the LLD by  $37.3 \pm 12.7\%$  (Fig. 5, *A* and *B*,  $n = 5$ ,  $P = 0.03$ ). The peak of the initial excitatory postsynaptic potential (EPSP), measured within first 20 ms, was not significantly reduced ( $15.5 \pm 8.7\%$ ,  $n = 5$ ,  $P = 0.13$ ) indicating that the effect of T-channel blockade was mainly due to reduction in the LLD (Fig. 5A). In three cells where APV (40  $\mu$ M) was subsequently added, the

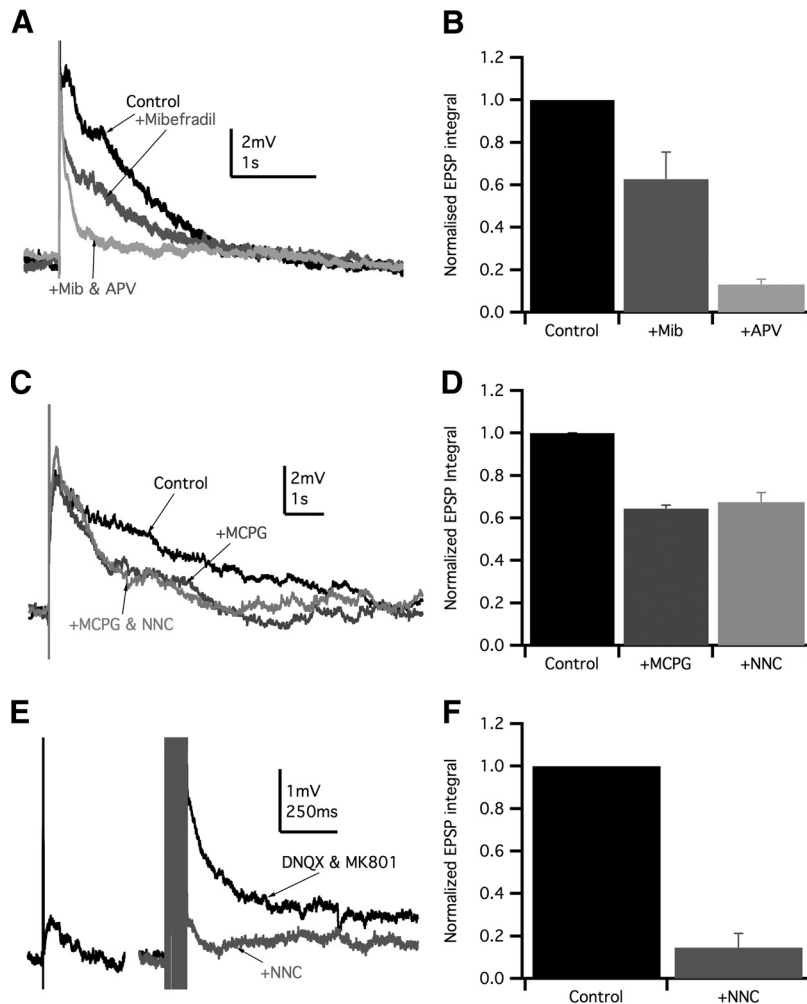


**FIG. 5.** mGluR activation is required for T-type channels to contribute to the olfactory nerve evoked long-lasting depolarizations (LLD). *A*: example of an olfactory nerve evoked LLD in control (black), after 10  $\mu\text{M}$  mibefradil (dark gray), and after mibefradil and 40  $\mu\text{M}$  APV (light gray). *B*: mibefradil caused a  $37.3 \pm 12.7\%$  ( $n = 5$ ,  $P = 0.03$ ) reduction in the normalized LLD integral, while subsequent APV application reduced the LLD integral to  $7.4 \pm 5.4\%$  of control values ( $n = 3$ ). *C*: example of an olfactory nerve evoked LLD in control (black), after 200  $\mu\text{M}$   $\alpha$ -methyl-4-carboxyphenylglycine (MCPG) (dark gray), and after MCPG and 50  $\mu\text{M}$  NNC 55-0396 (light gray). *D*: MCPG application reduced the LLD integral by  $35.5 \pm 1.5\%$  ( $P < 0.001$ ) and NNC55-0396 had no further effect ( $n = 5$ ). *E*, left: in the presence of 40  $\mu\text{M}$  DNQX and 20  $\mu\text{M}$  MK801, a single olfactory nerve stimulus is not very effective at evoking an isolated mGluR depolarization. A 100-Hz train of 10 stimuli to the olfactory nerve (black) result in a more robust depolarization, which is greatly attenuated by application of 50  $\mu\text{M}$  NNC 55-0396 (gray). *F*: NNC 55-0396 reduced the integral of the mGluR depolarization by  $85.4 \pm 6.7\%$  ( $n = 4$ ). N.B: all data recorded with 2 mM QX314 in the pipette with the resting membrane potential maintained at  $-64$  mV (junction potential corrected), examples and measurements are averages of  $\geq 4$  trials.

LLD was essentially abolished with the EPSP integral falling to  $7.4 \pm 5.4\%$  of control values (Fig. 5*B*).

These data indicate that T channels contribute to the LLD. However, is their activity during the LLD merely a result of depolarization from the AMPA/NMDA receptors or is their opening directly dependent on mGluR activation? With application of MCPG (200  $\mu\text{M}$ ) to block mGluRs, a  $35.5 \pm 1.5\%$  decrease in the LLD integral was observed (Fig. 5, *C* and *D*,  $P < 0.001$ ). Under these conditions, only T channels recruited solely by voltage would remain. Subsequent application of NNC 55-0396 (50  $\mu\text{M}$ ,  $n = 5$ ) had no effect, indicating that mGluR activation is necessary for T-channel activation during the LLD and that depolarization alone by distal currents does not directly open significant numbers of T channels.

Is T-channel upregulation the sole target of mGluR activation? Block of NMDA and AMPA receptors by perfusion with 40  $\mu\text{M}$  DNQX and 20  $\mu\text{M}$  MK801 during stimulation results in isolation of the mGluR-mediated depolarization. Under these conditions, mGluR receptors are not readily activated with a single stimulus (Fig. 5*E*) due to loss of recurrent excitation within the glomerulus required to saturate transporters (De Saint Jan and Westbrook 2007). However, a train of stimuli (10 pulses at 100 Hz, 30-s duty cycle) has been shown to release enough glutamate to activate mGluRs (Fig. 5*E*) (De Saint Jan and Westbrook 2007; Yuan and Knopfel 2006). In

four of seven cells tested, we were able to produce a mGluR response (all 7 displayed robust LLD in the absence of synaptic blockers). The decay time of the mGluR depolarization was  $715 \pm 351$  ms (measured as the time to 33% of peak amplitude,  $n = 4$ ). Application of 50  $\mu\text{M}$  NNC 55-0396 reduced the integral of the isolated mGluR depolarization to  $14.6 \pm 6.6\%$  of control ( $n = 4$ ,  $P = 0.001$ ), indicating that T channels are the major target of mGluR activation. This shows that mGluR activation alone is capable of generating depolarization by increasing T-channel activity.

#### Control of mitral cell firing by T-channel contribution to LLD

Sustained action potential firing results from the ON-evoked LLD (Fig. 6*C* control) (Aroniadou-Anderjaska et al. 1997; Ennis et al. 1996). Because T-type channel block reduces the integral of the LLD, we next determined the extent to which action potential firing would be reduced by loss of the T current. Application of T-type channel antagonists (mibefradil 10  $\mu\text{M}$ ,  $n = 5$  or NNC 55-0396 50  $\mu\text{M}$ ,  $n = 3$ ) reduced ON-evoked action potential firing by  $84.1 \pm 4.6\%$ . Reduction by NNC and mibefradil were similar, 85 and 81%, respectively, so the data were pooled. The number of spikes in each condition was determined from the average of 10 trials. In the cells that displayed early onset firing (5 of 8 cells), blocking

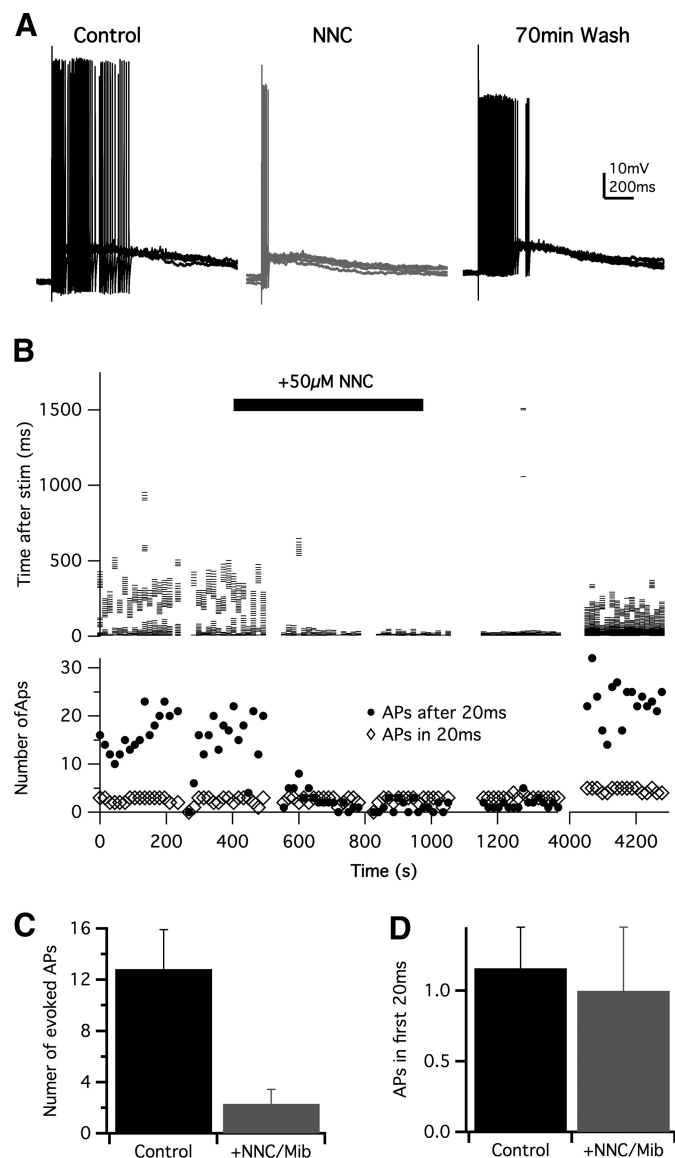


FIG. 6. T-type channels contribute to action potential output. *A*: olfactory nerve evoked responses in a mitral cell in control (black), in the presence of 50  $\mu\text{M}$  NNC 55-0396 (gray), and after a 70-min washout. *B*, *top*: a raster plot of the times of action potential occurrence during olfactory nerve stimuli delivered every 16 s, for the cell in *A*. *Bottom*: plot of the number of action potentials within the 1st 20 ms of stimulation (open diamonds) and after 20 ms (closed circles). *C*: T-type antagonists reduced total number of action potentials evoked per stimulus by  $84.1 \pm 4.6\%$  ( $n = 8$ ). *D*: T-type antagonists had little effect on the initial action potential rate in the 5 of 8 cells that showed early onset firing.

T-type channels had no effect on this firing in the first 20 ms after the stimulation (1.16 vs. 1.0,  $P = 0.52$ ,  $n = 5$ , Fig. 6, *D–F*). This is consistent with T-type channels predominantly contributing to the LLD rather than the initial phase of the EPSP, which is governed by AMPA receptors (De Saint Jan and Westbrook 2007). We were able to achieve reversal of the action potential suppression in one experiment with NNC 55-0396 (Fig. 6*D*) and in one with mibefradil; however, recovery required  $\geq 1$  h of rinsing consistent with previous reports of extremely slow wash-off for these compounds (Huang et al. 2004). The effects of T-type channel block are not explained by effects on the olfactory afferents as previous studies have shown that T-type

channel blockers have no effect on release from the ON (De Saint Jan and Westbrook 2007; Liu and Shipley 2008a).

## DISCUSSION

Mitral cell dendrites are endowed with many active conductances (Balu and Strowbridge 2007; Bischofberger and Jonas 1997; Kollo et al. 2008), support unattenuated back-propagating action potentials (Bischofberger and Jonas 1997) and initiate action potentials in their distal compartments in response to excitatory synaptic input (Chen et al. 1997). We show that mitral dendrites and tuft branches also possess T-type  $\text{Ca}^{2+}$  channels. They link  $[\text{Ca}^{2+}]$  to the subthreshold membrane potential and can drive  $\text{Ca}^{2+}$  entry during subthreshold oscillations, similar to those seen in vivo (Charpak et al. 2001). The T channels are robustly upregulated by group 1 mGluR activation in the primary dendrite. mGluR activation is required to recruit T channels during the ON-evoked LLD, where they contribute depolarizing current, increasing the spike output of mitral cells.

### $\text{Ca}^{2+}$ Channel subunits

LVA  $\text{Ca}^{2+}$  channels that show significant activation below  $-50$  mV include Cav3.x (T-type) and Cav1.3 (L-type) channels. The L-type blocker isradipine (500  $\mu\text{M}$ ) had no effect on the LVA  $\text{Ca}^{2+}$  current measured in voltage clamp or on the subthreshold  $\text{Ca}^{2+}$  entry measured optically. At this concentration, isradipine is more than sufficient to block the LVA L-type current mediated by Cav1.3 (Brandt et al. 2003; Koschak et al. 2001). The absence of Cav1.3 staining in juvenile mice (Yuan et al. 2004) is consistent with these physiological observations. L-type channels have been described in acutely dissociated mitral cells where they activated more positive than  $-30$  mV and were sensitive to low concentrations (5  $\mu\text{M}$ ) of dihydropyridines (Wang et al. 1996), which further suggests that L-type channels are not involved in the LVA  $\text{Ca}^{2+}$  current (Xu and Lipscombe 2001). The LVA current is sensitive to the T-type blockers mibefradil, NNC 55-0396 and 500  $\mu\text{M}$   $\text{Ni}^{2+}$ , indicating that Cav3 channels are responsible. The fact that 50  $\mu\text{M}$   $\text{Ni}^{2+}$  had no effect on the voltage onset rules out Cav3.2, which is highly sensitive to  $\text{Ni}^{2+}$  (Lee et al. 1999). As Cav3.3 staining is strong in the dendrites, it seems likely that Cav3.3 channels mediate this current, although a small contribution from Cav3.1 channels cannot be ruled out.

### T channels in mitral dendrites

Although T channels were observed in acutely isolated mitral cells (Wang et al. 1996), they have not been found in earlier slice studies. For example, using similar methods, Isaacson and Strowbridge (1998) found no evidence for T channels based on the lack of effect of 50  $\mu\text{M}$   $\text{Ni}^{2+}$ . At that time, it was assumed 50  $\mu\text{M}$   $\text{Ni}^{2+}$  was sufficient to block all T-type channels but Lee et al. (1999) subsequently showed that 50  $\mu\text{M}$   $\text{Ni}^{2+}$  is insufficient to block Cav3.1 and Cav3.3. We find that higher concentrations of  $\text{Ni}^{2+}$  are required to block the T channels in mitral cells, consistent with the immunohistochemistry for the Cav3.3 subtype. An additional reason T channels may have been overlooked is that the electrical impact they exert on mitral cells is subtle. This highlights an advantage of  $\text{Ca}^{2+}$  imaging combined with electrophysiology;

while current-clamp techniques detect the effect of summed inward and outward currents, Ca<sup>2+</sup> imaging specifically detects Ca<sup>2+</sup> influx, a fact exemplified in Fig. 3C. Ca<sup>2+</sup> imaging is sensitive to the integral of Ca<sup>2+</sup> influx so small currents that are difficult to detect electrophysiologically can often easily be detected by their effect on [Ca<sup>2+</sup>] if they persist for periods of a second or more (Awatramani et al. 2005).

Around the resting membrane potential (−65 to −55 mV for mitral cells), LVA T-type Ca<sup>2+</sup> channels typically have a region of overlap between their steady-state inactivation and activation curves, which is termed a “window current” (Randall and Tsien 1997). Our imaging and voltage-clamp data in Fig. 3 confirm that T channels in mitral cells have an active window current. Channels active at resting membrane potentials will contribute to the resting [Ca<sup>2+</sup>]. The imaging data from Fig. 4 shows that when T channels are upregulated by DHPG, a concomitant increase in resting [Ca<sup>2+</sup>] and Δ[Ca<sup>2+</sup>] on hyperpolarization is observed. When T channels are active, subthreshold changes in membrane potential drives changes in the resting [Ca<sup>2+</sup>]. This likely plays a role in the Ca<sup>2+</sup> oscillations seen in vivo (Chapman et al. 2001). Intriguingly, Cav3.3 channels overexpressed in NG108×15 cells induce synchronized [Ca<sup>2+</sup>] and voltage oscillations (Chevalier et al. 2006). In the accessory OB, sub-threshold voltage changes results in increases in [Ca<sup>2+</sup>] which produce transmitter release from mitral dendrites (Castro and Urban 2009). Considering the relatively large subthreshold voltage- and mGluR1-dependent [Ca<sup>2+</sup>] increases we observed in the mitral cells of the main OB, it is tempting to surmise that subthreshold release is also occurring. Alternatively or additionally, elevated [Ca<sup>2+</sup>] could potentiate action potential-evoked release as it does at many synapses including the calyx of Held, neuromuscular junction and hippocampal mossy fiber (Awatramani et al. 2005; Delaney and Tank 1994; Regehr et al. 1994).

### *mGluR regulation*

Mitral cells express mGluR1 but not mGluR5 (van den Pol 1995). Bath application of the group I agonist DHPG increased the [Ca<sup>2+</sup>] by increasing the activity of a T-type Ca<sup>2+</sup> channel at −64 mV. Furthermore, mGluRs activated by olfactory nerve stimulation increased T-channel activity resulting in a T-channel mediated depolarization (Fig. 5E). Interestingly, the increase in T-channel activity appeared highest in the distal dendrite and tuft, which is the location of the highest reported density of mGluR protein (van den Pol 1995), whereas at the soma where mGluR protein is low or absent, no DHPG-induced increase in Ca<sup>2+</sup> was observed. At resting membrane potentials, secondary dendrites appear to have LVA Ca<sup>2+</sup> current activity equal to or greater than that in the primary dendrites, but unlike the primary dendrite, there was no clear evidence for regulation by mGluR. This may reflect the presence in the secondary dendrites of a Cav3.3 splice variant that is active at RMP without the need for mGluR activation. The weaker Cav3.3 staining of the secondary dendrites would be expected due to their diameters being 2- to 10-fold thinner than the primary dendrites. Alternatively, our experiments cannot entirely rule out a contribution of Cav1.3 (LVA L-type), which although it is absent in the primary dendrite, may contribute to LVA Ca<sup>2+</sup> influx in the secondary dendrites.

mGluR1 activation primarily leads to signal transduction via the G<sub>α<sub>q</sub></sub> pathway, activating PLC and further downstream, PKC (Ferraguti et al. 2008). PKC activation increases the magnitude of all three Cav3 currents without changing kinetics or surface expression (Park et al. 2006). Therefore it is likely that the upregulation of the T channels seen here is via PKC activation (but see Hildebrand et al. 2007, who recently showed G<sub>α<sub>q/11</sub></sub> coupled to the M1 muscarinic receptor inhibits Cav3.3 channels through an as yet unidentified mechanism).

### *Mitral cell firing and the LLD*

In mitral cells, T-channel antagonists reduce the magnitude of the synaptic response and decrease spiking. A similar effect of T-channel antagonists is seen in external tufted cells; NNC 55-0396 reduces both the EPSP and the number of spikes with ON stimulation (Liu and Shipley 2008a). In tufted cells, however, T channels appear to be active all the time, contributing to their characteristic intrinsic oscillations (Liu and Shipley 2008b). In contrast, we show that in mitral cells, T channels have to be upregulated by mGluR activation to exert an effect.

Strong ON stimulation evokes an LLD in mitral cells that originates in the apical tuft dendrite (Carlson et al. 2000). It results from initial excitation by olfactory afferents that causes release of glutamate from tuft dendrites in the glomerulus, which in turn triggers recurrent excitation by mitral cells of the same glomerulus (Carlson et al. 2000; De Saint Jan and Westbrook 2007). The LLD is in part due to NMDA-R current while the remainder is dependent on mGluR1 (Carlson et al. 2000; De Saint Jan and Westbrook 2007). We show that the major target of mGluR activation is upregulation of T channels. This is consistent with the findings of Yuan et al. (2006), who showed large [Ca<sup>2+</sup>] increases in apical tuft dendrites in response to mGluR1 activation, which were not mediated by TRPC1.

Although the mechanisms governing the in vitro LLD are now well understood, it is not clear what role the LLD plays in an intact animal. The temporal properties of the LLD determine its potential roles. In vitro, the onset of the pharmacologically isolated mGluR depolarization is relatively rapid, occurring within ≤50 ms of the start of strong ON stimulation; exact quantification is difficult as it is obscured in the 100-ms train used to evoke it. The LLD persists for ≤12 s although 2–6 s is the typical duration in our experiments. In vivo mitral cells respond to odor stimulation by firing spikes on the crests of respiration-rate-determined membrane potential oscillations (Cang and Isaacson 2003; Schaefer et al. 2006; Sobel and Tank 1993). The relatively fast onset of the mGluR depolarization provides for the possibility that it contributes to respiration-locked depolarization on a cycle-by-cycle basis. Identification and discrimination of salient odors can occur within 100 ms (Uchida and Mainen 2003), so the relatively rapid onset of T-channel upregulation would be needed if it is involved in the fastest odor-processing events. The in vitro LLD lasts many seconds longer than a single oscillation (100–500 ms), indicating that the mGluR activation can potentially persist across respiratory cycles. Because the offset of the depolarization between respiratory cycles is faster than the decay of the LLD observed in vitro, additional mechanisms are likely to be involved in vivo. The down phase of the oscillation in vivo likely results from a combination of a pause in the olfactory

afferent excitation combined with inhibitory network actions of periglomerular and granule cells. Because both the NMDA-R and T-channel components are voltage-dependent, a local inhibitory drive would be efficient to attenuate the LLD. The persistence of the LLD *in vitro* may therefore reflect compromised inhibitory pathways and/or less efficient glutamate removal in an acute 300- $\mu\text{m}$  slice.

Our data show that reducing the magnitude of the ON-evoked LLD by blocking T channels significantly attenuates mitral cell firing. Because the mGluR response decays slowly relative to a sniff cycle, the membrane potential boost afforded by T channels can potentially persist across subsequent oscillations. This extra bed of depolarization would keep the mitral cells slightly more depolarized for subsequent up-phases and further enhance firing during and after odor application. Single-unit recordings performed by Matsumoto et al. (2009) demonstrated that mitral cell firing that often persists for  $\leq 80$  s after termination of an odor stimulus is due to mGluR1 activation. Thus sustained firing in mitral cells that depends on mGluR-activated T-channel may be important for maintaining an odor "trace" that facilitates the learning of odor associations with long delays between odor and reinforcing stimuli (Bordner and Spear 2006; Ferry et al. 2006) or to maintain odor-dependent motivational states.

#### General relevance

In our experiments,  $\sim 60\%$  of cells recorded in current clamp with normal ACSF showed membrane potential-dependent changes in  $[\text{Ca}^{2+}]$  around rest. However, virtually all cells we examined by voltage-clamp showed T-type current with high external TEA. In the *in vivo* studies of Charpak et al. (2001), the sensitivity of resting  $[\text{Ca}^{2+}]$  to membrane potential was seen in all cells where this was tested. In the TEA voltage-clamp solution, the membrane potential of surrounding cells will be depolarized, increasing release of glutamate, leading to a general upregulation of T channels. Consistent with this hypothesis, all mitral cells examined in normal ACSF displayed LVA  $\text{Ca}^{2+}$  influx in the presence of DHPG. *In vivo*, background neuronal activity may result in a tonic level of T-channel activation that is greater than that present in acute slices after several hours of perfusion with normal ACSF. This may explain a similar phenomenon seen in CA3 pyramidal neurons that also display strong dendritic Cav3.3 immunoreactivity (McKay et al. 2006). In voltage-clamp solutions (i.e., high TEA), CA3 neurons display a prominent T current (Avery and Johnston 1996), yet the contribution of T channels to resting  $[\text{Ca}^{2+}]$  is negligible when measured in normal saline (Magee et al. 1996).

Given the strong dendritic Cav3 immunoreactivity observed in many neurons that lack prominent electrophysiological signatures, including hippocampal pyramidal, cortical layer 5 pyramidal, cerebellar stellate, and Purkinje neurons (McKay et al. 2006), it is possible that Cav3 regulation by metabotropic receptors may provide a mechanism to locally influence dendritic processing in other neuronal types.

#### ACKNOWLEDGMENTS

Thanks are extended to D. Stuss for comments on the manuscript and to Drs. T. Snutch and G. Zamponi for supplying antibodies. Also thanks go to Dr. Ray Turner for sharing preliminary data on Cav3.3 antibody staining patterns.

#### GRANTS

This work was funded by the Canadian Institutes for Health Research Grant MOP 86743.

#### REFERENCES

- Aroniadou-Anderjaska V, Ennis M, Shipley MT. Glomerular synaptic responses to olfactory nerve input in rat olfactory bulb slices. *Neuroscience* 79: 425–434, 1997.
- Avery RB, Johnston D. Multiple channel types contribute to the low-voltage-activated calcium current in hippocampal CA3 pyramidal neurons. *J Neurosci* 16: 5567–5582, 1996.
- Awatramani GB, Price GD, Trussell LO. Modulation of transmitter release by presynaptic resting potential and background calcium levels. *Neuron* 48: 109–121, 2005.
- Balu R, Strowbridge BW. Opposing inward and outward conductances regulate rebound discharges in olfactory mitral cells. *J Neurophysiol* 97: 1959–1968, 2007.
- Bischofberger J, Jonas P. Action potential propagation into the presynaptic dendrites of rat mitral cells. *J Physiol* 504: 359–365, 1997.
- Bordner KA, Spear NE. Trace conditioning in 1-day-old rats. *Dev Psychobiol* 48: 58–70, 2006.
- Brandt A, Striessnig J, Moser T. CaV1.3 channels are essential for development and presynaptic activity of cochlear inner hair cells. *J Neurosci* 23: 10832–10840, 2003.
- Cang J, Isaacson JS. *In vivo* whole-cell recording of odor-evoked synaptic transmission in the rat olfactory bulb. *J Neurosci* 23: 4108–4116, 2003.
- Carlson GC, Shipley MT, Keller A. Long-lasting depolarizations in mitral cells of the rat olfactory bulb. *J Neurosci* 20: 2011–2021, 2000.
- Castro JB, Urban NN. Subthreshold glutamate release from mitral cell dendrites. *J Neurosci* 29: 7023–7030, 2009.
- Charpak S, Mertz J, Beaupaire E, Moreaux L, Delaney K. Odor-evoked calcium signals in dendrites of rat mitral cells. *Proc Natl Acad Sci USA* 98: 1230–1234, 2001.
- Chen WR, Midtgaard J, Shepherd GM. Forward and backward propagation of dendritic impulses and their synaptic control in mitral cells. *Science* 278: 463–467, 1997.
- Chevalier M, Lory P, Mironneau C, Macrez N, Quignard JF. T-type CaV3.3 calcium channels produce spontaneous low-threshold action potentials and intracellular calcium oscillations. *Eur J Neurosci* 23: 2321–2329, 2006.
- Delaney KR, Tank DW. A quantitative measurement of the dependence of short-term synaptic enhancement on presynaptic residual calcium. *J Neurosci* 14: 5885–5902, 1994.
- De Saint Jan D, Westbrook GL. Disynaptic amplification of metabotropic glutamate receptor 1 responses in the olfactory bulb. *J Neurosci* 27: 132–140, 2007.
- Desmaisons D, Vincent JD, Lledo PM. Control of action potential timing by intrinsic subthreshold oscillations in olfactory bulb output neurons. *J Neurosci* 19: 10727–10737, 1999.
- Djurisic M, Antic S, Chen WR, Zecevic D. Voltage imaging from dendrites of mitral cells: EPSP attenuation and spike trigger zones. *J Neurosci* 24: 6703–6714, 2004.
- Ennis M, Zimmer LA, Shipley MT. Olfactory nerve stimulation activates rat mitral cells via NMDA and non-NMDA receptors *in vitro*. *Neuroreport* 7: 989–992, 1996.
- Feng G, Mellor RH, Bernstein M, Keller-Peck C, Nguyen QT, Wallace M, Nerbonne JM, Lichtman JW, Sanes JR. Imaging neuronal subsets in transgenic mice expressing multiple spectral variants of GFP. *Neuron* 28: 41–51, 2000.
- Ferraguti F, Crepaldi L, Nicoletti F. Metabotropic glutamate 1 receptor: current concepts and perspectives. *Pharmacol Rev* 60: 536–581, 2008.
- Ferry B, Ferreira G, Traissard N, Majchrzak M. Selective involvement of the lateral entorhinal cortex in the control of the olfactory memory trace during conditioned odor aversion in the rat. *Behav Neurosci* 120: 1180–1186, 2006.
- Gire DH, Schoppa NE. Control of on/off glomerular signaling by a local GABAergic microcircuit in the olfactory bulb. *J Neurosci* 29: 13454–13464, 2009.
- Hildebrand ME, David LS, Hamid J, Mulatz K, Garcia E, Zamponi GW, Snutch TP. Selective inhibition of Cav3.3 T-type calcium channels by Galphaq/11-coupled muscarinic acetylcholine receptors. *J Biol Chem* 282: 21043–21055, 2007.

- Huang L, Keyser BM, Tagmose TM, Hansen JB, Taylor JT, Zhuang H, Zhang M, Ragsdale DS, Li M. NNC 55-0396 [(1S,2S)-2-(2-(N-[(3-benzimidazol-2-yl)propyl]-N-methylamino)ethyl)-6-fluoro-1,2,3,4-tetrahydro-1-isopropyl-2-naphthyl cyclopropanecarboxylate dihydrochloride]: a new selective inhibitor of T-type calcium channels. *J Pharmacol Exp Ther* 309: 193–199, 2004.
- Isaacson JS, Strowbridge BW. Olfactory reciprocal synapses: dendritic signaling in the CNS. *Neuron* 20: 749–761, 1998.
- Kim D, Song I, Keum S, Lee T, Jeong M, Kim S, McEnery MW, Shin H. Lack of the burst firing of thalamocortical relay neurons and resistance to absence seizures in mice lacking [alpha]1G T-type Ca<sup>2+</sup> channels. *Neuron* 31: 35–45, 2001.
- Klockner U, Lee JH, Cribbs LL, Daud A, Hescheler J, Peverzev A, Perez-Reyes E, Schneider T. Comparison of the Ca<sup>2+</sup> currents induced by expression of three cloned alpha subunits, alpha1G, alpha1H and alpha1I, of low-voltage-activated T-type Ca<sup>2+</sup> channels. *Eur J Neurosci* 11: 4171–4178, 1999.
- Kollo M, Holderith N, Antal M, Nusser Z. Unique clustering of A-type potassium channels on different cell types of the main olfactory bulb. *Eur J Neurosci* 27: 1686–1699, 2008.
- Koschak A, Reimer D, Huber I, Grabner M, Glossmann H, Engel J, Striessnig J. alpha 1D (Cav1.3) subunits can form I-type Ca<sup>2+</sup> channels activating at negative voltages. *J Biol Chem* 276: 22100–22106, 2001.
- Lee JH, Gomora JC, Cribbs LL, Perez-Reyes E. Nickel block of three cloned T-type calcium channels: low concentrations selectively block alpha1H. *Biophys J* 77: 3034–3042, 1999.
- Liu S, Shipley MT. Intrinsic conductances actively shape excitatory and inhibitory postsynaptic responses in olfactory bulb external tufted cells. *J Neurosci* 28: 10311–10322, 2008a.
- Liu S, Shipley MT. Multiple conductances cooperatively regulate spontaneous bursting in mouse olfactory bulb external tufted cells. *J Neurosci* 28: 1625–1639, 2008b.
- Magee JC, Avery RB, Christie BR, Johnston D. Dihydropyridine-sensitive, voltage-gated Ca<sup>2+</sup> channels contribute to the resting intracellular Ca<sup>2+</sup> concentration of hippocampal CA1 pyramidal neurons. *J Neurophysiol* 76: 3460–3470, 1996.
- Matsumoto H, Kashiwadani H, Nagao H, Aiba A, Mori K. Odor-induced persistent discharge of mitral cells in the mouse olfactory bulb. *J Neurophysiol* 101: 1890–1900, 2009.
- McKay BE, McRory JE, Molineux ML, Hamid J, Snutch TP, Zamponi GW, Turner RW. Ca(V)3 T-type calcium channel isoforms differentially distribute to somatic and dendritic compartments in rat central neurons. *Eur J Neurosci* 24: 2581–2594, 2006.
- McQuiston AR, Katz LC. Electrophysiology of interneurons in the glomerular layer of the rat olfactory bulb. *J Neurophysiol* 86: 1899–1907, 2001.
- Park JY, Kang HW, Moon HJ, Huh SU, Jeong SW, Soldatov NM, Lee JH. Activation of protein kinase C augments T-type Ca<sup>2+</sup> channel activity without changing channel surface density. *J Physiol* 577: 513–523, 2006.
- Price JL, Powell TP. The mitral and short axon cells of the olfactory bulb. *J Cell Sci* 7: 631–651, 1970.
- Randall AD, Tsien RW. Contrasting biophysical and pharmacological properties of T-type and R-type calcium channels. *Neuropharmacology* 36: 879–893, 1997.
- Regehr WG, Delaney KR, Tank DW. The role of presynaptic calcium in short-term enhancement at the hippocampal mossy fiber synapse. *J Neurosci* 14: 523–537, 1994.
- Schaefer AT, Angelo K, Spors H, Margrie TW. Neuronal oscillations enhance stimulus discrimination by ensuring action potential precision. *PLoS Biol* 4: e163, 2006.
- Schoppa NE, Westbrook GL. AMPA autoreceptors drive correlated spiking in olfactory bulb glomeruli. *Nat Neurosci* 5: 1194–1202, 2002.
- Sobel EC, Tank DW. Timing of odor stimulation does not alter patterning of olfactory bulb unit activity in freely breathing rats. *J Neurophysiol* 69: 1331–1337, 1993.
- Uchida N, Mainen ZF. Speed and accuracy of olfactory discrimination in the rat. *Nat Neurosci* 6: 1224–1229, 2003.
- van den Pol AN. Presynaptic metabotropic glutamate receptors in adult and developing neurons: autoexcitation in the olfactory bulb. *J Comp Neurol* 21: 253–271, 1995.
- Wang X, McKenzie JS, Kemm RE. Whole cell calcium currents in acutely isolated olfactory bulb output neurons of the rat. *J Neurophysiol* 75: 1138–1151, 1996.
- Xu W, Lipscombe D. Neuronal Ca(V)1.3alpha(1) L-type channels activate at relatively hyperpolarized membrane potentials and are incompletely inhibited by dihydropyridines. *J Neurosci* 21: 5944–5951, 2001.
- Yuan Q, Knopfel T. Olfactory nerve stimulation-evoked mGluR1 slow potentials, oscillations, and calcium signaling in mouse olfactory bulb mitral cells. *J Neurophysiol* 95: 3097–3104, 2006.
- Yuan Q, Mutoh H, Debarbieux F, Knopfel T. Calcium signaling in mitral cell dendrites of olfactory bulbs of neonatal rats and mice during olfactory nerve stimulation and beta-adrenoceptor activation. *Learn Mem* 11: 406–411, 2004.